RSC Advances

PAPER

View Article Online
View Journal | View Issue

Cite this: *RSC Adv.*, 2025, **15**, 29500

Study on the thermal radiation tolerance characteristics of lithium-ion batteries

Mengbai Ma, *[ab] Shiqiang Wang,[ab] Hui Jiang,[ab] Xiaolei Bi,[ab] Guanlin Peng,[ab] Bin Tao[ab] and Yingjie Zhang[ab]

With the extensive use of lithium-ion batteries (LIBs) in electrochemical energy storage systems and electric vehicles, their safety concerns have gradually emerged. Once LIBs undergo thermal runaway (TR), they can potentially trigger fire and explosion accidents, presenting substantial safety hazards. Regarding the issue that LIBs may experience TR due to external fires or other high-temperature conditions, the study of their thermal runaway tolerance characteristics under different degrees of external thermal radiation triggering conditions is of great significance in guiding the safe design and operation of LIB systems. Tests on lithium iron phosphate (LFP) and nickel manganese cobalt (NCM) batteries under the influence of different degrees of thermal radiation were conducted to obtain the typical phenomena, thermal radiation tolerance characteristics and tolerance zones of the abovementioned two LIBs after thermal runaway. Experimental results demonstrate that the thermal radiation tolerance thresholds of the NCM batteries and LFP batteries are 1.158 kW m^{-2} and 1.88 kW m^{-2}, respectively, suggesting that LFP batteries exhibit superior thermal radiation tolerance compared to NCM batteries. Furthermore, prediction models for the duration of external thermal radiation exposure tolerated by NCM and LFP batteries were developed based on the experimental datasets; the models demonstrated a high goodness-of-fit (R^2 = 0.96166 and 0.97698, respectively), validating their predictive accuracy. This research can provide guidance for the safety and protection of LIBs under external thermal radiation conditions (such as external fire and direct sun), which is of great significance for their safe operation.

Received 21st May 2025
Accepted 5th August 2025

DOI: 10.1039/d5ra03552j

rsc.li/rsc-advances

1 Introduction

Lithium-ion batteries, characterized by their elevated energy density and extended cycle life, are extensively utilized in applications such as electric vehicles and large-scale energy storage systems.[1,2] Nonetheless, as the energy density of lithium-ion batteries escalates, their safety performance has significantly deteriorated, resulting in numerous related safety incidents. The internal components of these batteries are combustible and volatile. When subjected to thermal, electrical, or mechanical abuse,[3] intricate chemical reactions can be triggered, generating excessive heat, which leads to thermal runaway, potentially causing fires and explosions.[4–6] Currently, certain researchers have concentrated their investigations on thermal runaway in LIBs, primarily examining gas generation,[7–9] heat production,[10–12] fire incidents,[13–16] and explosive behaviors.[17,18] Nevertheless, the majority of current research concentrates on the behaviors after thermal runaway. In practical scenarios, the extrinsic factors that induce thermal runaway should be quantified as well. Regarding thermal runaway-triggering conditions, overcharging and heating are the most common methods used to induce thermal runaway in LIBs. The specific methods of heating LIBs include direct heat conduction and thermal radiation. According to some research reports, in direct heating, the power of the heating plate significantly impacts the thermal runaway and its propagation characteristics in LIBs.[19,20] A low-power heating plate enhances the top heating effect and accelerates the propagation of thermal runaway in the battery, while a high-power heating plate weakens the top heating effect, thereby reducing the propagation speed of thermal runaway. Huang Z. *et al.*[21] triggered thermal runaway in 38 Ah lithium batteries using direct heating and overcharging methods and observed the heat and gas production behaviors during thermal runaway. The specific operation for heating triggering thermal runaway involved using a heating plate with a fixed power of 300 W and 400 W in direct contact with the battery for heating. Additionally, a round electric heater was placed 85 mm away from the battery to simulate the heat radiation condition.[22] Q. Wang *et al.*[23] used a 3 kW electric heater as an external heat radiation source for a 50 Ah $LiFePO_4$/graphite battery to trigger thermal runaway, and then the surface temperature, combustion behavior, heat release rate, flame temperature and mass loss rate were obtained.

[a]State Key Laboratory of Chemical Safety, Qingdao, 266104, China. E-mail: mamb.qday@sinopec.com
[b]SINOPEC Research Institute of Safety Engineering Co., Ltd, Qingdao, 266104, China

However, in most real-world scenarios, thermal runaway in LIBs under external overheating conditions is usually caused by thermal radiation. A possible threat occurs in regular gas stations that are equipped with electric vehicle charging stations. For instance, in the event of a fire in the refueling area, the heat generated by burning gasoline may affect the LIBs in electric vehicles being charged through thermal radiation, potentially triggering thermal runaway in the LIBs. Although a considerable amount of research has been conducted, the primary focus of research has been the characteristics of batteries post-thermal runaway, while quantitative studies on the triggering conditions for thermal runaway in lithium-ion batteries remain relatively scarce. Thus, to address this knowledge gap, a series of experiments was conducted to investigate the thermal runaway triggering characteristics of batteries under different thermal radiation intensities. The distance between the thermal radiation generator and the LIBs was adjusted to create a thermal radiation field around the LIBs, and tests were conducted to obtain the thermal runaway trigger temperature and time, phenomena, surface temperature variations, and fire behaviors of the LIBs. Two types of LIBs (LFP-60Ah and NCM-42Ah) were prepared in this test. A quantitative analysis of the tolerance characteristics of the LIBs under diverse thermal radiation intensities was carried out. For the first time, the thermal radiation threshold that typical commercial LIBs can tolerate was determined, which offers crucial data support for the safety and protection of LIBs under the influence of thermal radiation.

2 Experimental

2.1 Battery samples

As the two most widely used commercial LIBs, NCM and LFP batteries were selected as the research objects in this experiment. The details of these cells are listed in Table 1.

To investigate the influence of different thermal radiation intensities on the tolerance characteristics of LIB thermal runaway, tests of the thermal radiation field at varying distances from a fixed thermal radiation source were conducted. Firstly, a far-infrared heating screen was selected as a stable thermal radiation generator, with the power of the generator set to 4.5 kW. The front of the thermal radiometer was directly facing the thermal radiation generator, and the distance between them was set to d, where d had values of 0.5 cm, 2 cm, 5 cm, 10 cm, 15 cm, 20 cm, 25 cm, 30 cm, 40 cm, 50 cm, 70 cm, and 90 cm, respectively. At each distance, two sets of thermal radiometers were tested simultaneously, and the average value was taken as the true thermal radiation intensity value. The corresponding relationship between distance and heat radiation intensity is shown in Table 2.

Table 2 Distribution of the thermal radiation field

Distance (cm)	Thermal radiation intensity value (kW m^{-2})
0.2	3.5154
0.5	3.28526
1	3.02649
2	2.77028
5	2.52676
10	2.23494
20	1.57809
30	1.15888
40	0.91655
50	0.69409
70	0.41711
90	0.25176

This value was then connected to a data acquisition device for real-time transmission of signals to obtain the distribution of thermal radiation intensity at different distances. The experimental system is shown in Fig. 1(a), and the actual layout is shown in Fig. 1(b). Fig. 1(c) illustrates the distribution of the thermal radiation field at different distances between the thermal radiation generator and the battery. The intensity of thermal radiation decreases with an increase in distance and shows a significant negative correlation with the square of the distance.

As depicted in Fig. 2, thermal radiation was employed to trigger thermal runaway in lithium-ion batteries (LIBs). Firstly, the LIBs to be tested were charged to the target SOC. Subsequently, the large surface of each battery was positioned directly facing the thermal radiation generator. During the placement, it was ensured that the safety valve of each battery was located directly above to prevent displacement during the material ejection process that occurs after the battery experiences thermal runaway.

K-type thermocouples were arranged at the center points of the front and back surfaces of the battery to record the surface temperature of a single LIB. The temperature data was collected and transmitted *via* a connected data acquisition device. Considering safety, the data acquisition device was placed in a central control room. A video camera was positioned 3–4 meters behind the single battery cell to record the key stages and phenomena of LIB thermal runaway.

This study delved into the impacts of different thermal radiation intensities, battery types, and SOC on the tolerance characteristics of LIBs. To realize enhanced readability, the

Table 1 Battery parameters

Type of LIB	Electrode material	Capacity (Ah)	Cutoff voltage (V)	Operating voltage (V)	Weight (g)	Format	Dimensions (length × width × height mm)
LFP	$LiFePO_4$–graphite	60	3.2	2.5–3.65	1395	Rectangle	135 × 29.3 × 185
NCM	$LiNi_{0.6}Mn_{0.2}Co_{0.2}O_2$–graphite	42	3.7	2.8–4.25	890	Rectangle	147 × 27 × 97

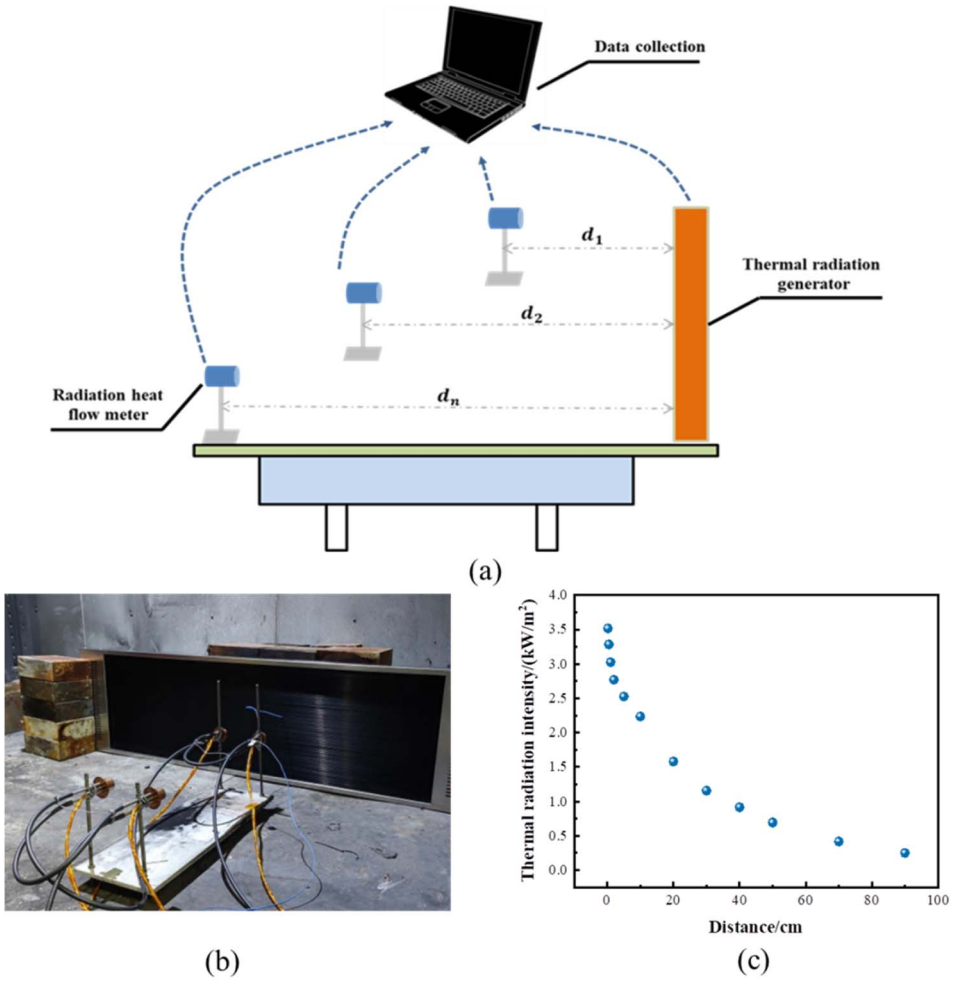

Fig. 1 Thermal radiation field test platform layout (a) schematic, (b) real diagram, (c) correspondence between thermal radiation and distance.

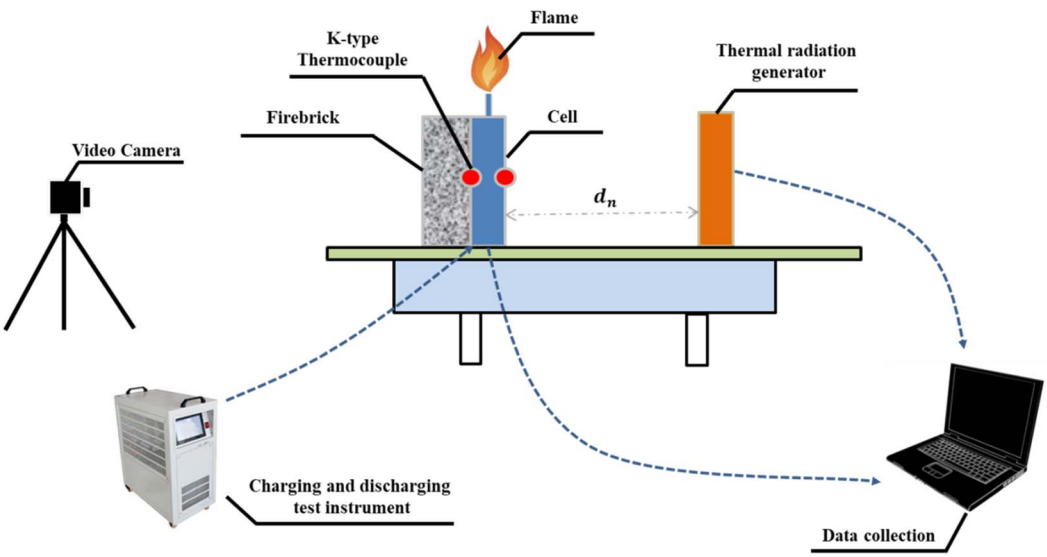

Fig. 2 Thermal radiation field test platform layout.

Table 3 Experimental parameters

Number	Type of LIBs	Distance (cm)	SOC
1	LFP	0.5, 2, 5, 10, 15, 20, 25, 30, 40, 50, 70, 90	100%
2	NCM	0.5, 2, 5, 10, 15, 20, 25, 30, 40, 50, 70, 90	100%
3	LFP	2	75%
4	LFP	2	50%
5	LFP	2	25%
6	LFP	2	0

distance between the battery and the thermal radiation generator was adopted to represent the varying thermal radiation intensities. To achieve the purpose of variable control, all parameters except those being measured were kept constant. The settings of the test parameters are presented in Table 3.

3 Results and discussion

3.1 Analysis of the temperature rise characteristics and phenomena

The records from the video cameras showed that there were significant differences in the thermal runaway phenomena between LFP and NCM under the influence of thermal radiation.

3.1.1 NCM batteries. The rising temperature curves of all the NCM batteries at different distances in the experiment are presented in Fig. 3. Owing to the diverse intensities of thermal radiation, each battery displayed distinct phenomena at various positions relative to the thermal radiation source, and these phenomena conformed to certain regular patterns. Specifically, at different distances (corresponding to varying heat radiation intensities), some LIBs exhibited only a temperature rise without thermal runaway. In the case of the LIBs that experienced thermal runaway, although the triggering time varied, it followed a distinct trend, where shorter distances corresponded to shorter triggering times. In the range of 0.5 cm to 25 cm, all the LIBs underwent thermal runaway. Correspondingly, at distances greater than or equal to 30 cm, no thermal runaway occurred.

When the distance between the battery and the heat radiation source exceeded than 30 cm, corresponding to a heat radiation intensity of less than 1.158 kW m^{-2}, the temperature of the NCM gradually reached a stable state after rising to a certain value. Moreover, the stable temperature value decreased as the heat radiation intensity diminished. To investigate the threshold of heat radiation tolerance by NCM, the battery was continuously exposed to heat for 24 h at a distance of 30 cm from the heat radiation source. The test results shown in Fig. 4 indicated that the surface temperature of the battery reached 147.8 °C at the end of the test. At 15 h into the experiment, the rate of temperature rise had stabilized at 0.5 °C h^{-1}. In this experiment, even though the temperature of the surface had already exceeded the decomposition temperature of the SEI film (80–120 °C) in 3.5 h, the tested battery did not experience thermal runaway under a heat radiation intensity of 1.158 kW m^{-2} after 24 h. Although the NCM experienced temperature elevation under thermal radiation exposure, its substantial distance from the radiation source resulted in limited heat absorption. This yielded a reduced heat generation rate within the battery. Consequently, by maintaining a persistent state where the heat generation remained below the dissipation capacity, the battery achieved thermal stability. This phenomenon aligns with the observations in the LFP battery.

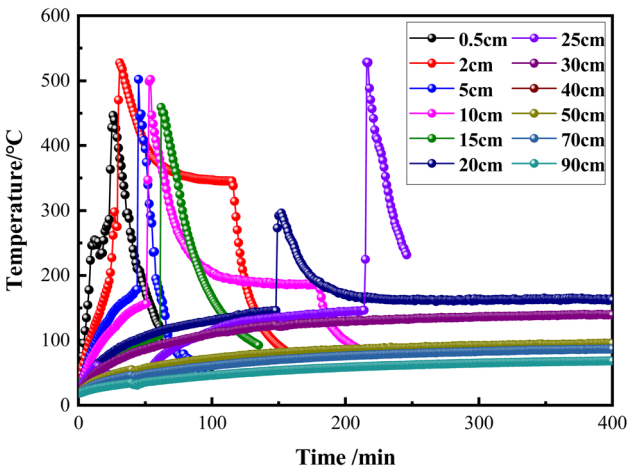

Fig. 3 Temperature rise curves of NCM at different distances.

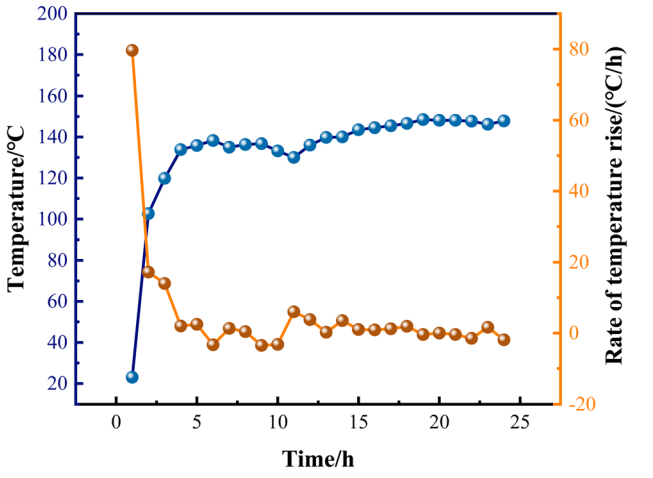

Fig. 4 Temperature characteristics of NCM under a heat radiation intensity of 1.158 kW m^{-2} after enduring for 24 h.

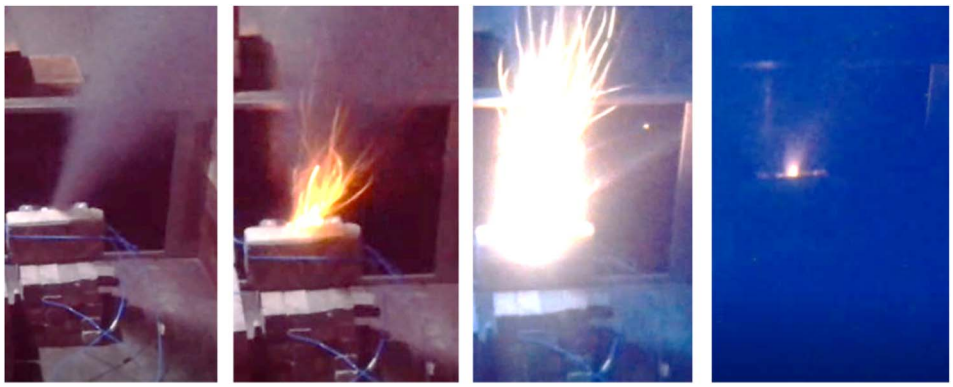

Fig. 5 Thermal runaway phenomenon in NCM.

As depicted in Fig. 5, all the NCM batteries exposed to a heat radiation intensity greater than 1.158 kW m^{-2} underwent thermal runaway during the experiment. In the early stages of thermal runaway development, the NCM swelled due to internal gas production. As the heat radiation continued to affect the battery, the temperature rose rapidly, and there was a clear correlation between the rate of temperature rise and the triggering time of thermal runaway with the intensity of heat radiation. With the continuous increase in internal gas production, the safety valve of the battery opened, ejecting a small amount of electrolyte and visible smoke. Approximately 30 s after the safety valve opened, a conical jet flame emerged at the pressure relief opening. As thermal runaway continued, the combustion grew increasingly intense, with the surface temperature of the battery peaking at around 500 °C. Eventually, the flames gradually died out, the temperature dropped rapidly, and the thermal runaway phenomenon came to an end.

3.1.2 LFP batteries. The rising temperature curves of all the LFP batteries at different distances in the experiment are presented in Fig. 6. When the distance between the battery and the heat radiation source was greater than or equal to 15 cm, meaning the heat radiation intensity was less than 1.88 kW m^{-2}, the temperature of the LFP batteries gradually reached a stable state after rising to a certain value, and the stable temperature value decreased as the heat radiation intensity decreased.

To investigate the threshold of heat radiation tolerance of LFP, the batteries were continuously exposed to heat for 24 h at distances of 15 cm and 20 cm from the heat source, corresponding to heat radiation intensities of 1.88 kW m^{-2} and 1.57 kW m^{-2}, respectively. As illustrated in Fig. 7, the test results revealed that the surface temperatures of the batteries reached 210.8 °C and 193.6 °C at the end of the experiment. Approximately 6 h into the experiment, the temperature increased slowly at a rate of 3 °C h^{-1}. Starting from the 16th hour, the rate of temperature rise of the LFP batteries fluctuated at around 0 °C h^{-1}, indicating that the temperature had gradually stabilized.

In contrast to NCM, LFP did not generate an open flame after thermal runaway in the tests at various distances. Fig. 8 illustrates a partial screenshot of the battery temperature rise curve when the battery was placed at distances of 0.5 cm and 2 cm from the heat radiation source, with the relative time zone ranging from 0–60 min. As an example, the temperature characteristics of the batteries under these two conditions were demonstrated.

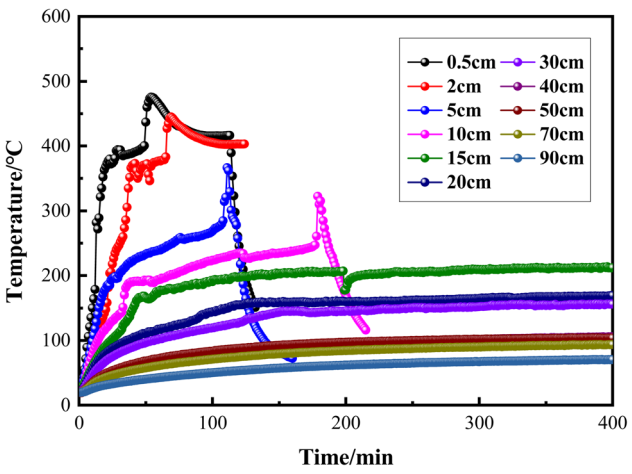

Fig. 6 Temperature rise curves of LFP at different distances.

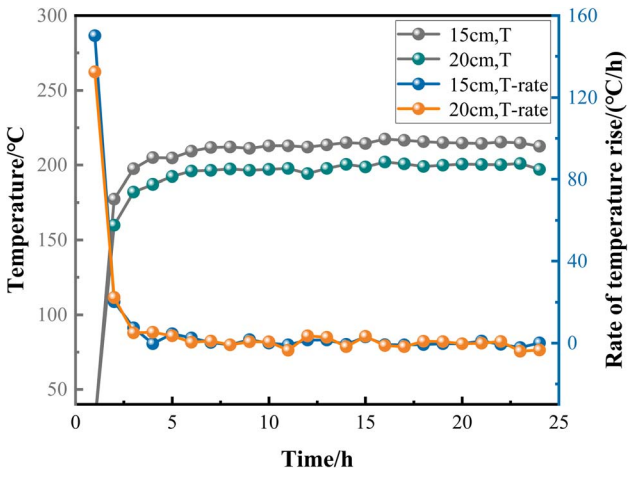

Fig. 7 Temperature characteristics of LFP under heat radiation intensities of 1.88 kW m^{-2} and 1.57 kW m^{-2} after enduring for 24 h.

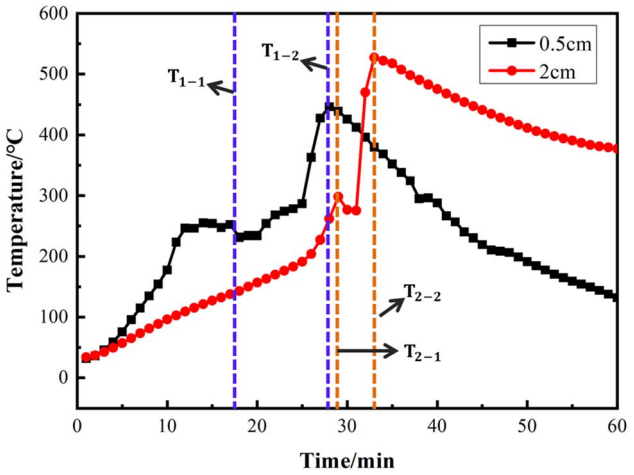

Fig. 8 Partial temperature characteristics of LFP under heat radiation intensities of 1.88 kW m^{-2} and 1.57 kW m^{-2}.

During the exposure of LFP to thermal radiation, the initial observable phenomenon was a temperature increase. The rate of temperature rise became more pronounced as the distance from the heat radiation source decreased. As the surface temperature of the battery reached 200 °C during this process, it was accompanied by the decomposition of the SEI film, a reaction between the negative electrode and the electrolyte, and melting of the separator. Consequently, the batteries started to generate gas continuously inside, which led to an increase in the internal pressure of the batteries and causing them to swell and deform significantly. At the moments T_{1-1} and T_{2-1} for the two groups of batteries, respectively, the safety valve opened. The escaping flue gas dissipated some heat, resulting in a slight drop in temperature.

As shown in Fig. 9(a), since thermal runaway had not yet occurred at this point, the concentration of smoke was relatively low. About 5 to 10 min after the valve opened, due to the continuous influence of the heat radiation source, the temperature rise rate of the LFP batteries increased sharply. Thermal runaway occurred at moments T_{1-2} and T_{2-2}, with a large amount of smoke being instantaneously ejected. In a short time, the smoke filled the entire space, as shown in Fig. 9(b)–(d).

3.2 Analysis of tolerance characteristics under the influence of thermal radiation field

In this experiment, the point with a temperature rise rate greater than 1 °C s^{-1} was taken as the starting point of thermal runaway. The starting times of all the thermal runaway-batteries were sequentially determined, which represented the tolerance time of the LIB under the corresponding thermal radiation intensity. All the data were plotted as a scatter plot, and a model fitting was performed on the processed data. The fitting results are shown in Fig. 10.

The "tolerance time-thermal radiation intensity" models for LFP and NCM can be obtained separately. The calculation model for the change in tolerance time of NCM with thermal radiation intensity is shown in eqn (1-1), as follows:

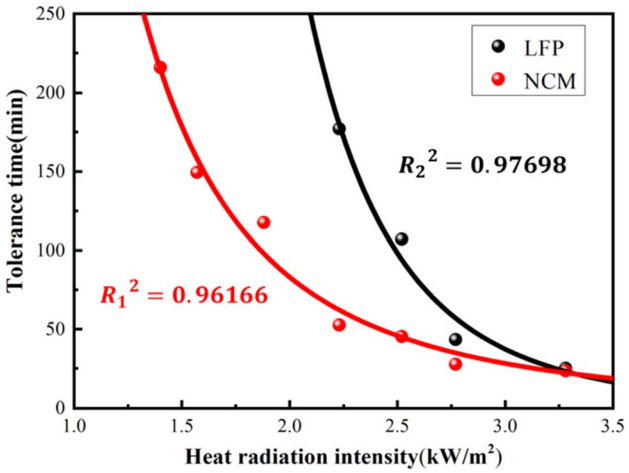

Fig. 10 Thermal radiation-endurance time data fitting curve of the lithium battery.

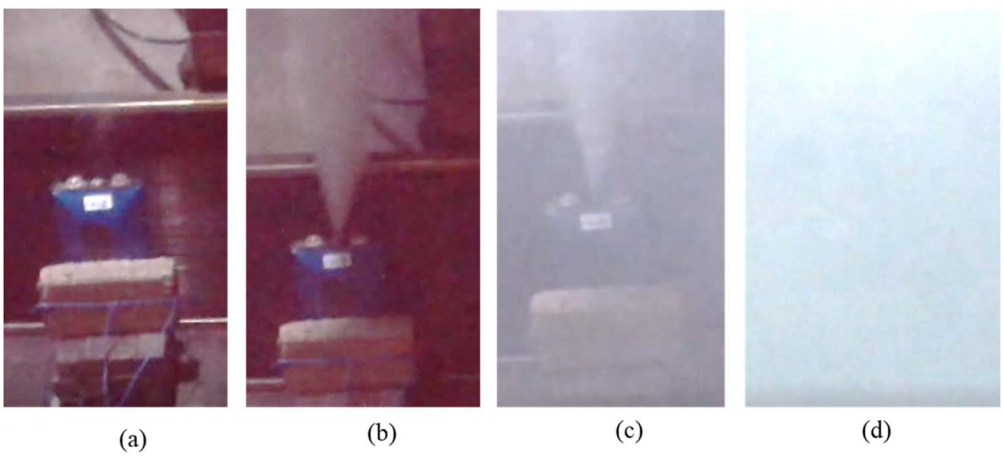

Fig. 9 Thermal runaway phenomenon in LFP (a) LFP without thermal runaway, (b) LFP safety valve opening, (c) rapid smoke ejection, (d) entire space filled with smoke.

$$t_1 = 525 \times \hat{q} - 2.661,\ q > 1.158 \quad (1\text{-}1)$$

The calculation model for the change in tolerance time of LFP with thermal radiation intensity is shown in eqn (1-2), as follows:

$$t_2 = 12651 \times \hat{q} - 5.302,\ q > 1.88 \quad (1\text{-}2)$$

where q (kW m^{-2}) is the thermal radiation intensity received by the LIB and t (min) is the tolerance time of the LIBs under the corresponding thermal radiation intensity. The goodness of fit R_1^2 for NCM is 0.96166, and the goodness of fit R_2^2 for LFP is 0.97698, indicating that the fitting model has good credibility. As can be seen in Fig. 10, the two types of LIBs show a similar trend. However, due to the better thermal stability of LFP, its tolerance performance is superior to that of NCM.

In the case of the LIBs that experienced thermal runaway, the temperature corresponding to the point where the temperature rise rate is greater than 1 °C s^{-1} is defined as the trigger temperature for thermal runaway. This temperature, along with the stable temperature of the LIBs that did not experience thermal runaway, is plotted in Fig. 11. As can be seen in Fig. 11, for the LIBs that did not experience thermal runaway, when the test duration was set to 12 h, the stable temperature value increases with an enhancement in thermal radiation. Once the LIBs maintain a stable state, they will not experience thermal runaway even if they are continuously exposed to thermal radiation for 12 h. Based on the data characteristics, it can be divided into three zones in Fig. 11, *i.e.*, the tolerance zone for NCM, the tolerance zone for LFP, and the thermal runaway zone. Points A and B are the critical points for the thermal runaway of LFP and NCM, respectively. Due to the better thermal stability of LFP, its tolerance zone area is larger than that of NCM. Additionally, under the same thermal radiation intensity, the trigger temperature for LFP is higher, indicating that it is more difficult for LFP to experience thermal runaway compared to NCM.

3.3 Analysis of the impact of SOC on heat radiation tolerance characteristics

LFP were charged to the SOC values of 75%, 50%, 25%, and 0%, respectively. After charging, the target battery was placed 2 cm away from the heat radiation source. As shown in Fig. 12, at the

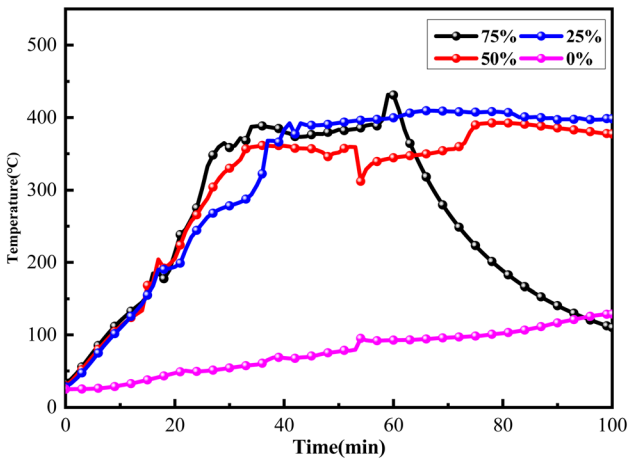

Fig. 12 Thermal radiation temperature rise curves of LFP at various SOC values.

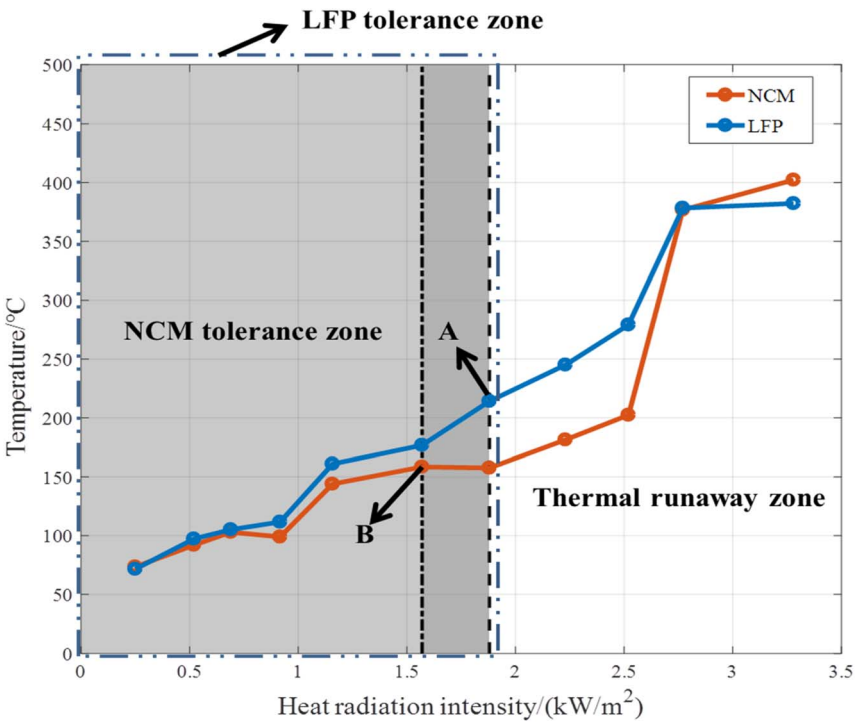

Fig. 11 Heat radiation tolerance zone.

Table 4 Key moments of LFP at different SOC values

SOC	Valve opening time (min)	Thermal runaway initiation time (min)
75%	18.7	25.95
50%	19.38	29.8
25%	19.95	36.4
0%	53.2	—

same distance, thermal runaway occurred in LFP with SOC values of 75%, 50%, and 25%. However, when the SOC was 0%, LFP only exhibited a stable temperature rise and did not experience thermal runaway.

The extraction of critical time points from the thermal radiation temperature rise data at 2 cm for LFP with different SOC values is shown in Table 4. At the same distance, as the SOC increases, the time for the safety valve in LFP to open and the thermal runaway initiation time may accelerate, but there is no significant overall difference. When the SOC is at 0%, the safety valve of the LIB opens after being heated for 53.2 min, but no thermal runaway behavior occurs during the subsequent testing process.

4 Conclusion

This work systematically investigates the characteristics of thermal radiation effects on two mainstream LIBs. Through experimental research on the tolerance characteristics of LIBs under different thermal radiation intensities, battery types, and SOC values, the thermal radiation tolerance characteristics of NCM and LFP batteries are identified, relevant tolerance prediction models and tolerance zones are established, and the thermal runaway phenomena and behaviors of the two types of LIBs are discussed. The main conclusions are as follows:

(1) There are significant differences in the phenomena after thermal runaway between NCM and LFP batteries. The main manifestations of thermal runaway in NCM after exposure to thermal radiation are "safety valve opening – gas eruption – jet fire," while the main manifestations of LFP are "safety valve opening – small amount of gas eruption – large amount of gas eruption". Therefore, NCM shows a higher fire risk compared to LFP, LFP only ejects gas after thermal runaway, and if thermal runaway occurs in an airtight energy storage cabin or battery swap cabin, the risk of gas explosion for it is much higher than that of NCM. Additionally, the experimental data indicate that the interval between valve opening and complete thermal runaway in the LFP batteries is 5–10 min, which can be used as the "golden time" for thermal runaway early warning. Various methods should be adopted in this period for early warning to prevent accidents.

(2) Analysis of the experimental data shows that under the influence of thermal radiation, LFP exhibits better tolerance performance than NCM. The thermal radiation tolerance thresholds for the above-mentioned two types of batteries are 1.88 kW m^{-2} and 1.158 kW m^{-2}, respectively. Below these thresholds, the batteries will not experience thermal runaway after 24 h of continuous thermal radiation.

(3) In the experiments, the "thermal radiation intensity-tolerance time" data points for both types of batteries show similar trends, and the models conform to the distribution of power functions. Due to the better thermal stability of LFP, its tolerance zone is larger than that of NCM. Furthermore, under the same thermal radiation intensity, the trigger temperature of LFP is higher, indicating that it is more difficult for LFP to experience thermal runaway compared to NCM. Overall, based on these experimental results, the tolerance characteristics of LFP are superior to that of NCM.

(4) SOC has a certain impact on the tolerance performance of LIBs. Under a certain thermal radiation intensity, due to the lower activity of batteries with a low SOC, the tolerance time increases as the SOC decreases. At 0% SOC, LFP did not experience thermal runaway after 6 h of continuous thermal radiation.

Conflicts of interest

There are no conflicts to declare.

Data availability

The data supporting the findings of this study are available from the corresponding author upon reasonable request.

References

1 J. Wen, D. Zhao and C. Zhang, An overview of electricity powered vehicles: Lithium-ion battery energy storage density and energy conversion efficiency, *Renewable Energy*, 2020, **162**, 1629–1648.
2 J.-M. Tarascon and M. Armand, Issues and challenges facing rechargeable lithium batteries, *Nature*, 2001, **414**, 359–367.
3 W. Gao, X. Li, M. Ma, *et al.*, Case study of an electric vehicle battery thermal runaway and online internal short-circuit detection, *IEEE Trans. Power Electron.*, 2020, **36**, 2452–2455.
4 J. Hong, Z. Wang, C. Qu, *et al.*, Investigation on overcharge-caused thermal runaway of lithium-ion batteries in real-world electric vehicles, *Appl. Energy*, 2022, **321**, 119229.
5 B. Mao, H. Chen, Z. Cui, T. Wu and Q. Wang, Failure mechanism of the lithium ion battery during nail penetration, *Int. J. Heat Mass Transfer*, 2018, **122**, 1103–1115.
6 V. Ruiz, A. Pfrang, A. Kriston, *et al.*, A review of international abuse testing standards and regulations for lithium ion batteries in electric and hybrid electric vehicles, *Renewable Sustainable Energy Rev.*, 2018, **81**, 1427–1452.
7 L. Yuan, T. Dubaniewicz, I. Zlochower, *et al.*, Experimental study on thermal runaway and vented gases of lithium-ion cells, *Process Saf. Environ. Prot.*, 2020, **144**, 186–192.
8 A. W. Golubkov, S. Scheikl, R. Planteu, *et al.*, Thermal runaway of commercial 18650 Li-ion batteries with LFP and NCA cathodes-Impact of state of charge and overcharge, *RSC Adv.*, 2015, **5**, 57171–57186.

9 A. W Golubkov, D. Fuchs, J. Wagner, *et al.*, Thermal-runaway experiments on consumer Li-ion batteries with metal-oxide and olivin-type cathodes, *RSC Adv.*, 2014, **4**, 3633–3642.
10 A. Perea, A. Paolella, J. Dube, *et al.*, State of charge influence on thermal reactions and abuse tests in commercial lithium-ion cells, *J. Power Sources*, 2018, **399**, 392–397.
11 K. Sascha, K. P Birke and R. Kuhn, Fast Thermal Runaway Detection for Lithium-Ion Cells in Large Scale Traction Batteries, *Batteries*, 2018, **4**, 16.
12 P. Liu, C. Liu, K. Yang, *et al.*, Thermal runaway and fire behaviors of lithium iron phosphate battery induced by over heating, *J. Energy Storage*, 2020, **31**, 101714.
13 Y. Fu, S. Lu, K. Lu, *et al.*, An experimental study on burning behaviors of 18650 lithium ion batteries using a cone calorimeter, *J. Power Sources*, 2015, **273**, 216–222.
14 M. Chen, J. Liu, Y. He, *et al.*, Study of the fire hazards of lithium-ion batteries at different pressures, *Appl. Therm. Eng.*, 2017, **125**, 1061–1074.
15 P. Ping, Q. S. Wang, P. F. Huang, *et al.*, Study of the fire behavior of high-energy lithium-ion batteries with full-scale burning test, *J. Power Sources*, 2015, **285**, 80–89.
16 X. Liu, Z. Wu, S. I. Stoliarov, *et al.*, Heat release during thermally-induced failure of a lithium ion battery: Impact of cathode composition, *Fire Saf. J.*, 2016, **85**, 10–22.
17 A. R. Baird, E. J. Archibald, K. C. Marr, *et al.*, Explosion hazards from lithium-ion battery vent gas, *J. Power Sources*, 2020, **446**, 227257.
18 A. O. Said, C. Lee and S. I. Stoliarov, Experimental investigation of cascading failure in 18650 lithium ion cell arrays: Impact of cathode chemistry, *J. Power Sources*, 2020, **446**, 227347.
19 C. Jin, Y. Sun, J. Yao, *et al.*, No thermal runaway propagation optimization design of battery arrangement for cell-to-chassis technology, *eTransportation*, 2022, **14**, 100199.
20 C. Jin, Y. Sun, H. Wang, *et al.*, Model and experiments to investigate thermal runaway characterization of lithium-ion batteries induced by external heating method, *J. Power Sources*, 2021, **504**, 230065.
21 Z. Huang, J. Liu, H. Zhai, *et al.*, Experimental investigation on the characteristics of thermal runaway and its propagation of large-format lithium ion batteries under overcharging and overheating conditions, *Energy*, 2021, **233**, 121103.
22 P. Huang, Q. Wang, K. Li, *et al.*, The combustion behavior of large scale lithium titanate battery, *Sci. Rep.*, 2015, **5**, 7788.
23 Q. Wang, P. Huang, P. Ping, Y. Du and K. Li, Combustion behavior of lithium iron phosphate battery induced by external heat radiation, *J. Loss Prev. Process Ind.*, 2017, **47**, 961–969.